Energy Storage Materials 22 (2019) 168–178

Contents lists available at ScienceDirect

Energy Storage Materials

journal homepage: www.elsevier.com/locate/ensm

An ion conductive polyimide encapsulation: New insight and significant performance enhancement of sodium based P2 layered cathodes

Karthikeyan Kaliyappan [a,b], Gaoran Li [b], Lin Yang [a,**], Zhengyu Bai [a], Zhongwei Chen [b,*]

[a] School of Chemistry and Chemical Engineering, Key Laboratory of Green Chemical Media and Reactions, Ministry of Education, Henan Normal University, Xinxiang, 453007, China

[b] Department of Chemical Engineering, University of Waterloo, 200 University Avenue West, Waterloo, Ontario, N2L 3G1, Canada

ARTICLE INFO

Keywords:
Sodium ion batteries
P2-type electrodes
Polyimide
Surface modification
Ion-conductive coating

ABSTRACT

It is essential to stabilize the surface of P2 layered cathode materials at high cut-off voltages (>4.3 V) in order to construct high-energy sodium ion batteries (SIB) that are promising for commercial application. When the voltage exceeds 4.3 V, large volume changes due to phase transitions and active species dissolution affect the structural stability of high voltage cathodes. In this study, we report a novel method of enhancing the electrochemical cycling performance of P2-type $Na_{2/3}(Mn_{0.54}Ni_{0.13}Co_{0.13})O_2$ (NNMC) materials through ion-conductive polyimide (PI) encapsulation. The electrochemical performance of ultrathin PI coated NNMC (PI-NNMC) is one of the best reported in the literature among layered cathodes in terms of cyclic stability (82% after 100 cycles at 0.16 A g^{-1}) at a high voltage range between 2 and 4.5 V, compared to the pristine (46%) and Al_2O_3-coated NNMC (70%). At high current (5C), the NNMC-PI electrode demonstrates superior cyclability by retaining 70% of its capacity after 500 cycles. The ultrathin PI layer possesses excellent surface protection, high ionic conductivity (vs Al_2O_3 coating) and facile ion transport, thus enabling a fast and durable redox electrochemistry in NNMC materials for high-performance sodium storage above 4.3 V.

1. Introduction

Lithium ion batteries (LIBs) are promising energy storage systems for large-scale applications such as electrical vehicles (EV) and hybrid electrical vehicles (HEV) due to their high energy density and excellent electrochemical stability. However, there are still many shortcomings of the LIBs that should be seriously concerned such as the cost, toxicity, safety issues, availability of lithium raw materials, and unfavorable high-temperature performance [1]. Sodium ion batteries (SIBs) are a promising alternative to LIBs, as sodium is one of the most abundant element on earth crust and also much cheaper compared to lithium metal [2,3]. The intercalation/deintercalation of Na-ions in the host material was first reported in 1980 and the primary research on sodium rechargeable batteries was summarized by Abraham [2,3]. In the case of anode, numerous potential candidates such as carbonaceous materials, metal oxides, alloys, sulfides, Ti-based intercalation anodes are being investigated so far [4–6]. Among them, the carbonaceous materials with more disordered structure are demonstrated to deliver viable capacity and stability [5,6]. However, these disorder carbons have very low operating voltage (near 0 vs Na+/Na), rising the safety issues due to the formation of sodium dendrite at high current rates [5,6]. Hence, the preparation of carbon materials with heteroatoms (N or S) had been proposed as high rate and stable anode materials for SIB [7]. In addition, the composite of carbon and alloy materials such as Sb, Sn and Bi have also been demonstrated as alternative negative electrode for SIB application. However, these alloy composite materials have very low specific capacity and poor rate performance. In addition, the thin film of Sn-Sb, Sn-Ge, Sb-Si and Sn-Ge-Sb are reported to deliver the capacity ranges between 600 and 800 mAh g^{-1} with long term cyclability in SIB configuration [8–10]. Recently, Ti-based anodes ($Na_2Ti_3O_7$ and $NaTiO_2$) have been intensively investigated as alternative anodes for SIBs [11–14]. The main drawbacks of these anodes are the low capacity and inadequate rate capability due to the low conductivity of both electron and Na-ions. Hence, many efforts have been devoted to find better negative electrode to fabricate high performance SIBs.

In contrast, several sodium intercalation cathodes, for instance, layered transition metal oxides, fluorophosphates, hexacyanoferrates, Na_2FePO_4F, $Na_4M_3(PO_4)_2(P2O_7)$ (M = Fe/Co), Na_2FeP2O_7 and tunnel

* Corresponding author.
** Corresponding author.
E-mail address: zhwchen@uwaterloo.ca (Z. Chen).

https://doi.org/10.1016/j.ensm.2019.07.010
Received 21 March 2019; Received in revised form 28 June 2019; Accepted 8 July 2019
Available online 11 July 2019

structural materials were reported with considerable sodium storage capability [15,16]. However, these materials displayed poor ability to store sodium ions into their structures and severe capacity fading upon cycling [17,18]. Unlike their Li^+ analogue, layered Na^+ host materials do not suffer from cation mixing between sodium and transition metal ion layers due to the larger atomic radius of sodium (Na^+ - 1.02 Å) than that of lithium (Li^+ - 0.76 Å), leading to a well-developed layered structure [19]. In general, layered Na based intercalation materials could be mainly categorized as O3- and P2-type structure, in which Na-ions are occupying at octahedral and prismatic sites, respectively [20]. Among the structural types, P2-type materials are known to exhibit better electrochemical characteristics due to its high diffusion rate of Na-ion and inhibited slab-gliding [20]. The phase changes between O3- and P2-types could be attributed to the gliding of MO_2 sheets at ambient temperature [19,20]. Much research effort has been devoted to developing P2 type layered materials due to their better electrochemical performance [21–23]. In spite of showing stable electrochemical Na-ion intercalation/deintercalation behavior at low current densities, P2 cathodes experience severe capacity fading and poor rate performance due to the complicated phase transformation reaction and the active species dissolution during charge/discharge (C/DC) process, which severely restricts their practical application [21].

In order to improve their electrochemical performance, development of layered oxides with transition metal mixtures have been investigated extensively for SIB [1]. This enables improved Na^+ storage performance than that of its native compound, although capacity decay still persists [24,25]. Several layered oxides including P2-$Na_{0.45}Ni_{0.22}Co_{0.11}Mn_{0.66}O_2$, P2-$Na_{0.85}Li_{0.17}Ni_{0.21}Mn_{0.64}O_2$, $Na_{0.67}(Mn_{0.65}Co_{0.2}Ni_{0.15}]O_2$, P2-type $Na_{2/3}Ni_{1/3}Mn_{2/3-x}Ti_xO_2$ and P2-$Na_x[Fe_{1/2}Mn_{1/2}]O_2$ were investigated and reported elsewhere [20,26–30]. Unfortunately, the main disadvantage of these materials is that they cannot tolerate deep charging above 4.3 V (*vs* Na/Na^+). When charged above ~4.3 V, the capacity of these layered oxide degrades rapidly as a result of irreversible structural changes, restricting the complete capacity utilization of active materials. Despite showing favorable features such as low cost and stable performance, SIBs with low working cell voltages are inadequate for practical use especially with EVs and HEVs. Since the accumulation of energy in an electrochemical device is directly proportional to the cell voltage, the energy density of SIB can be increased by enhancing the operating voltage and capacity. Apart from that, the poor rate capability of above-mentioned electrode materials mainly originates from their low electronic conductivity and the formation of dense solid-electrolyte interfacial layer (SEI) during cycling [31–34]. Therefore, it is essential to develop advanced high-voltage electrode materials with highly conductive and robust electrode/electrolyte interface for future SIB applications.

Although cation doping strategy could help to enhance the structural stability, the doped cathodes still exhibits poor rate performance and cyclic performance at high cut-off voltages [30,35,36]. Surface coating with carbon or metal oxide are effective ways to enhance the cyclic stability of cathode materials at high voltages [37–39]. Recently, various metal oxide coatings (such as Al_2O_3, ZrO_2 and TiO_2 as protective layer) have been demonstrated to improve the cyclic performance of P2 layered cathodes at high cut-off voltages, which prevented the surface from electrolyte attack and accommodated the volume changes during the structural transformations [40–42]. Among metal oxides, electrodes coated with ultra-thin Al_2O_3 layer showed improved cyclic stability while ZrO_2 coated samples displayed better rate perfroamcne [22,23]. The cycle stability enhancement at high voltage from metal oxide coatings is still inadequate for practical application due to its low electrical and ion conductive properties [22–24]. In addition, metal oxides are often discontinuously deposited between the particles, thus acting as an inert layer to ionic conduction. Therefore, complex and expensive coating process like atomic layer deposition (ALD) are required to form uniform metal oxide coatings, but this technique only coats the electrode surface instead of materials themselves [22,23]. Of late, polymer encapsulation/hybrid composite have been extensively studied to improve the performance of LIBs in both the cathodic and anodic regions [43–45]. However, these strategies have not been fully explored in SIB cathodes, particularly at high cut-off voltages (>4.3 V).

These advantages motivate us to design a novel surface protection based on the encapsulation of uniform ion-conductive polymer electrolyte layer (IPEL) on P2 layered cathode materials. Unlike carbon or metal oxide coatings, the IPEL is considered as a promising surface protection technique as it not only increases the stability of the cathode but also forms a continuous ionic conductive coating layer on active materials [25]. Polyimide (PI) is being used in various application including fuel cells, membranes, microelectronics and electrode materials for energy storage, due to its excellent ionic conductivity and thermal stability [46–53]. In this study, we utilized polyimide (PI) as an IPEL to boost the Na-ion storage performance of P2-type layered $Na_{2/3}(Mn_{0.54}Ni_{0.13}Co_{0.13})O_2$ (NNMC) cathodes at high voltages (>4.3 V). The PI IPEL on NNMC was generated from the thermal imidization of polyamic acid (PAA) synthesized from oxydianiline (ODA)/pyromellitic dianhydride (PMDA) polymerization reaction [31]. The remarkable film-forming capability of PAA along with the strong affinity towards cathode surfaces result in ultrathin uniform formation of ionic conductive PI IPEL on NNMC surface [31,32]. To the best of our knowledge, this is the first ever report to fabricate IPEL on SIB intercalation cathode materials. Precisely, emphasis is focused on the comparison of the electrochemical performance of IPEL coated NNMC with pristine and Al_2O_3 coated NNMC electrode to understand the influence of IPEL on the electrochemical performance of SIBs including discharge capacity, rate performance and cyclability at high operating window of 2–4.5 V.

2. Experimental

2.1. Preparation of P2-NNMC

Initially, P2-type NNMC powders are prepared using a sol-gel method described as follows: stoichiometric amount of acetates of sodium, manganese, nickel and cobalt were dissolved in deionized water and stirred for 30 min. Then, chelating agent solution (citric acid, CA) as was slowly added into the above metal solution. The solution was heated under constant stirring at 120 °C until a viscous transparent gel is obtained. The resulting gel precursors were decomposed at 400 °C for 4 h and then heated at 850 °C for 12 h in air with intermediate grinding to obtain high crystalline layered materials.

2.2. ALD of Al_2O_3 on NNMC electrode

A layer of Al_2O_3 on NNMC electrode surface was performed at 120 °C using an ALD system (Thermal Gemstar 6XT, Arradiance, LLC, USA) in which Trimethylaluminum (TMA) and H_2O were used as the precursor and oxidizer, respectively. The detailed electrode preparation and ALD procedure could be found in our previous report [42]. Ten ALD of Al_2O_3 were performed on NNMC electrodes for half-cell measurements while 84 cycles of ALD cycles were used on NNMC powder for morphological characterizations.

2.3. PI coating on NNMC

PI IPEL on NNMC was developed from the thermal imidization reaction of PAA. The 5 wt% of PAA solution was prepared by dissolving PMDA and ODA reactants in dimethylacetamide (DMAC) solvent. Typically, ODA and PMDA solids were dissolved in 0.1 M of DMAC solvent and stirred for 12 h. The molar ratio of PMDA to ODA was fixed at 1. The 1 wt% PAA solution was prepared separately from the above mixture by diluting with DMAC solvent. 1 g of pristine NNMC powders were mixed with 1 wt% PAA solution and then stirred for 2 h. All reactions were taken place in an argon filled glove box. The mixture of PAA and NNMC solution were filtered and dried at 40 °C for 12 h under vacuum. Finally,

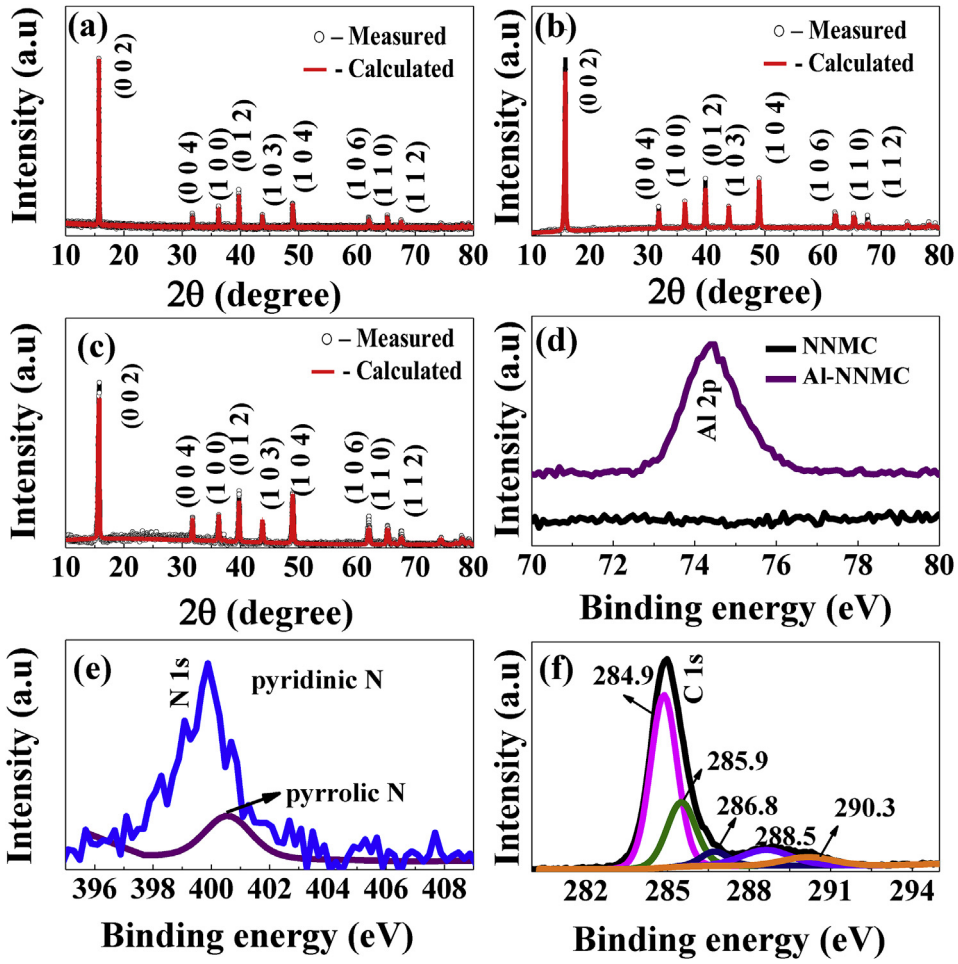

Fig. 1. Rietveld refinement of (a) NNMC, (b) Al-NNMC and (c) PI-NNMC powders, XPS of (d) Al 2p of Al-NNMC power, (e) and (f) N 1s and C 1s of PI-NNMC powders.

the conversion of PAA to IPEL was carried out by multi-step thermal imidization process, which consisted of heating at 60 °C for 120 min → 120 °C for 60 min → 200 °C for 60 min → 300 °C for 60 min → 400 °C for 10 min under argon atmosphere. Finally, Al_2O_3 (10 ALD cycles) and PI coated NNMC powers were named as Al-NNMC and PI-NNMC, respectively.

2.4. Characterizations

The crystalline structures of the prepared powders were characterized by using X-ray diffraction (XRD, Miniflex 600, RIgaku, Japan) with Cu Kα radiation. The surface morphology of the powder was observed in a field emission scanning electron microscope (FE-SEM, LEO Zeiss 1550, Switzerland) and high-resolution transmission electron microscope (HR-TEM, JEOL 2010 FEG). Thermogravimetric analysis (TGA) was conducted using a thermal analyzer system (TA instrument Q500) at a rate of 5 $^{o}Cmin^{-1}$ with an alumina crucible as the sample holder. X-ray photoelectron spectroscopy of C-NMB was conducted using Thermo Scientific Theta Probe, USA. Fourier transform infrared (FT-IR) spectroscopy was conducted on an IRPresitge-21 spectrometer (Japan). The electrochemical measurements of the prepared samples were performed in CR2032 type coin cell. The cathodes for electrochemical analysis were prepared by casting a slurry containing 70 wt% of NNMC/Al-NNMC/PI-NNMC materials, 20 wt% Ketjenblack as conductive additive and 10 wt% Teflonized acetylene black binder on stainless steel current collector and dried in a vacuum oven at ~80 °C overnight. The testing cells were constructed in an argon-filled glove box by pressing a composite cathode, porous polypropylene separator (Celgard 2400) and sodium metal counter electrode with 1 M $NaClO_4$ in ethylene carbonate (EC)/diethyl carbonate (DEC) (1:1 v/v) as the electrolyte solution. The mass loading of the electrodes is differing from 3 to 5 mg. Electrochemical impedance spectroscopy (EIS) and cyclic voltammetry (CV) studies were carried out in an electrochemical analyzer (Bio-Logic, France). The C/DC studies were conducted within a voltages range of 2–4.5 V at various current densities (1C = 160 mA g^{-1}) using a Land battery test system at ambient temperature.

3. Results and discussion

Fig. 1a presents the Rietveld refinement of pristine NNMC prepared through the sol-gel method at 850 °C with its crystal structure shown in Fig. S1. The XRD pattern owns well-developed, sharp, and intense peaks that reflects the high crystalline nature of the synthesized NNMC powders. It is well known that the Na^+ in prismatic sites are occupied between the MO_2 sheets and these Na^+ in prismatic sites had two different types namely Na_f and Na_e, which are sharing the edge with MO_6 octahedra to form layered structure [35]. The crystalline peaks are indicative of hexagonal structure with a $P6_3/mmc$ (JCPDS No. 194) space group [20,29,35]. The refinement fitting results along with the atomic occupancies for all metal ions are presented in Table S1. The stochiometric amount of sodium used in the preparation closely matches with the refined value of 0.63 for the NNMC sample. In addition, the majority of Na ions in NNMC occupy in Na (2) site, which is electrostatically more favorable than other Na sites [40].

The Rietveld refinement analysis of Al-NNMC and PI-NNMC are presented in Fig. 1b and c respectively. It is clear that all patterns are

Table 1
Crystallographic Parameters for the NNMC, Al-NNMC and PI-NNMC samples.

Sample	a (Å)	c (Å)	Cell Volume (Å^3)	Fitting factor R_p (%)
NNMC	2.859	11.210	77.298	9.08
Al-NNMC	2.855	11.211	77.296	8.45
PI-NNMC	2.853	11.212	77.297	8.94

identical and no substantial difference in the XRD patterns is noted between pristine, Al_2O_3- and PI-coated materials [33]. The lattice parameters are also calculated and shown in Table 1. The calculated lattice parameters for all samples are found to be very close and in good accordance with the previously reported values for P2 layered structure [20–25]. The XRD patterns also reveal that the surface modifications (Al_2O_3 or PI coating) do not deteriorate the structure of NNMC sample [23,24]. High crystallinity of cathode materials is vital for good electrochemical cycling performance and structural stability during battery cycling [27,29].

XPS spectroscopy was employed to analyze the presence of coating materials on the NNMC surface. Fig. 1c presents the XPS spectrum of Al 2p of alumina coated NNMC, in which the Al-NNMC sample shows an Al 2p peak at 74.5 eV while the pristine NNMC does not displays Al peak, confirming the presence of alumina coating layer on the surface of NNMC powders. On the other hand, the XPS of PI-NNMC in Fig. 1e and f reveal the presence of carbon and nitrogen functional groups on the surface of the PI-NNMC particles. The N 1s spectrum exhibits two characteristic peaks at 398.2 eV and 400.3 eV, which could be assigned to pyridinic (N1) and pyrrolic (N2) nitrogen, respectively [35]. The core-level C 1s spectra of PI-NNMC in Fig. 1f displays the sp [2] C-C, C-OH (hydroxy), C=O (carbonyl) and O=C-OH (carboxyl), and π- π* functional groups at binding energy of 284.9, 285.9, 286.8, 288.5 and 290.3 eV, respectively [54]. PI coating layer with nitrogen incorporation not only act as conductive agent to further enhance the conductivity of NNMC electrode, but also alleviate the pulverization of the NNMC materials and stabilizes the electrode structure during the electrochemical cycling process [31,32]. Moreover, the higher electronegativity and smaller atomic diameter of nitrogen atom along with carbon effectively facilitate the interaction between the sodium ions and coating layer [35,55]. These unique features of PI make it a favorable coating layer for achieving high capacity even at fast Na-ion insertion/reinsertion rates. Thus, enhanced cycling stability would be expected for the PI-NNMC electrode when compared to pristine and Al_2O_3 coated NNMC electrode.

Fig. 2a presents the Na 1s spectra of pristine and surface modified NNMC materials, all of which exhibit a peak centered at 1071.22 eV, demonstrating the +1 oxidation state of sodium [18]. The XPS spectra of Ni 2p in Fig. 2b displays four characteristic peaks centered at 855.09, 861.31, 872.91 and 880.12 eV. The peaks positioned at 855.09 eV (Ni $2p_{3/2}$) and 872.91 eV (Ni $2p_{1/2}$) are attributed to the characteristic features of elemental Ni whereas the peaks at 861.31 and 880.12 eV are indexed to the shakeup peaks of elemental Ni [56]. On the other hand, the XPS spectrums of Co 2p and Mn 2p in Fig. 2c and d, respectively, exhibit characteristic peaks at 780.32, and ~642 eV, respectively. This clearly reveals that the Mn has the valence state between +3 and + 4, and Co is +3 and + 2, respectively [25]. It is worth noting that while the peak positions of Co 2p and Ni 2p for Al-NNMC and PI-NNMC (Fig. 2b and c) are consistent with pristine NNMC, the Mn 2p spectrum of NNMC-PI in Fig. 2d shows a clear lower energy peak shift from 642.6 eV to 641.9 eV, demonstrating the electron adsorption by the Mn atom during the polymer coating. Zhang et al. proposed that the charge transfer between electron donor (C=O and benzene ring in PI) and electron acceptor species (surface Mn^{4+} in NNMC) results in the weak Mn(III) … benzine ring and Mn(III)···O interactions [46]. This partial reduction of Mn from Mn^{4+} to Mn^{3+} during PI coating is potentially favorable to improving electrochemical cyclic stability and the rate performance of the pristine NNMC materials [25].

The SEM image of NNMC powder prepared with CA at 850 °C is presented in Fig. 3a. The as-prepared NNMC exhibits clearly flake-shaped smooth particles with uniform particle size and distributions without any

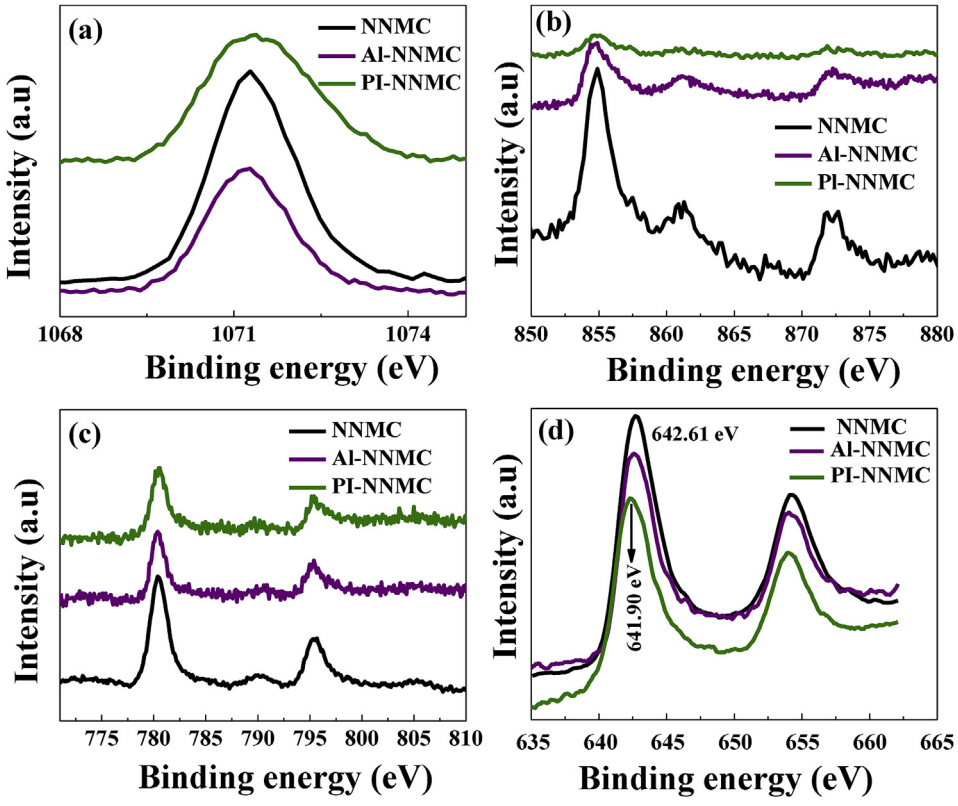

Fig. 2. XPS spectra of (a) Na 1s, (b) Ni 2p, (c) Co 2p and (d) Mn 2p of pristine and surface modified NNMC cathode materials.

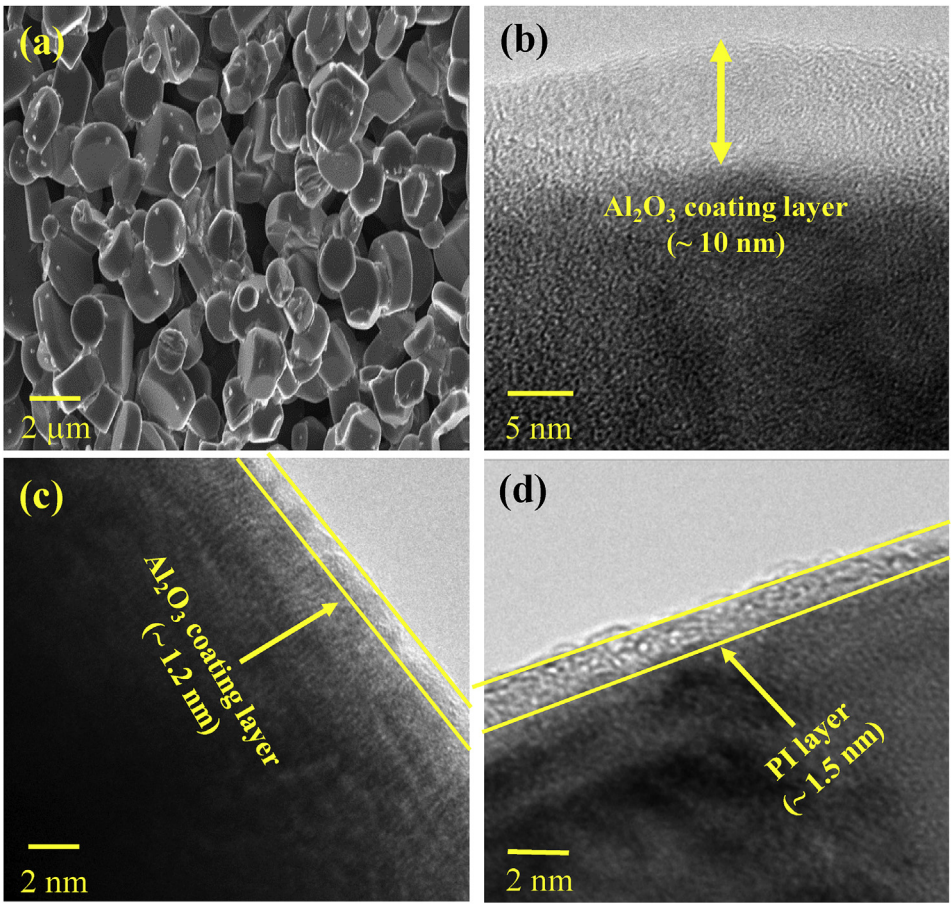

Fig. 3. (a) SEM image of NNMC prepared using sol-gel method at 850 °C for 12 h. TEM images of (b) and (c) Al_2O_3 coated on NNMC powders using 84 and 10 cycles of ALD, respectively and (d) TEM image of PI coated NNMC powders.

agglomeration benefiting from the addition of citric acid chelating agent. It is worth mentioning that the CA not only reduces the particles agglomeration but also facilitates uniform crystal growth and high surface area particles, which is important for better contact between the particles and high rate performance. The BET surface area of NNMC is measured to be about 2.32 $m^2 g^{-1}$. The relatively high surface area of NNMC sample is possibly resulted from the thermal decomposition of CA, which releases CO and CO_2 and forms large volume of voids during the synthesis. Additionally, high crystalline nature and large exposed contact area of NNMC could enable an enhanced utilization of active materials for electrochemical reaction [29]. Importantly, uniform sized particles also improves the contact between active material, conductive additives and current collector, and hence, improve the Na-ion diffusion rate and conductivity profiles within the electrode as well [32,33]. The EDX mapping of NNMC, Al-NNMC and PI-NNMC in Figs S2, S3 and S4, respectively, which clearly demonstrate the uniform distribution of Na, Ni, Mn and Co in the particles. In addition, Figs. S3 and S4 confirm the presence of Al on Al-NNMC surface and C and N on PI-NNMC samples, which further demonstrate the uniform distribution of coating layer on NNMC particles.

Fig. 3b illustrates the high resolution TEM image of NNMC particle coated with 84 cycles of ALD of Al_2O_3 layer. It could be noted that the 84 cycles of ALD can produce uniform Al_2O_3 layer with about ~9.5 nm thickness on NNMC particle surface, which equals to ~0.12 nm per cycles. In our work, we have done 10 ALD cycles of Al_2O_3 deposition on NNMC electrode surface, resulting an ultrathin uniform Al_2O_3 (~1.2 nm thickness) coating layer on the electrode as presented in Fig. 3c. In contrast, the TEM image of the as-developed PI-NNMC in Fig. 3d exhibits an amorphous uniform thin PI coating layer (~1.5 nm) on the surface of the NNMC powders. It is vital to develop an ultrathin protection layer on the NNMC surface to avoid harmful electrolyte side reactions and active species dissolution into the electrolyte [24,36]. Further, the metal oxide/PI coating layer could also accommodate the volume expansion arisen from the P2-O2 phase transformation during the Na-ion insertion/reinsertion process and provide structural stability for enhanced rate performance of the parent materials [40–42,57].

To further confirm the presence of PI coating on NNMC surface, FTIR measurement was carried out and the spectra is illustrated in Fig. S5a. The FTIR spectra of PI-NNMC clearly exhibits a peak at ~1782 cm^{-1} referring to the C=O (asymmetric stretch) of PI, while no peaks can be found between 1630 and 1650 cm^{-1} [46,49]. This is consistent with the previously reported that the polyamic acid shows C=O bond at around 1650 cm^{-1} and it shifts to ~ 1780 cm^{-1} after successful imidization process [48,49,58]. In addition, a sharp intense peak at 1319 cm^{-1} can be identified as the stretching vibration of the imide C-N group in PI film [25]. These results collectively confirm the successful imidization of polyamic acid and the formation of PI film on NNMC surface [27,38]. The Raman analysis was performed to prove the occurrence of imidization process rather than the carbonation during the thermal treatment as presented in Fig. S5b in the supporting information. The absence of peaks corresponding to the D-band for at ~1345 cm^{-1} or G-band at ~1596 cm^{-1} in Fig. S5b clearly demonstrates that no carbonization of polyamic acid occurred on the surface of NNMC particles at 400 °C.

The schematic illustration of polymerization process and coating layer of PI-NNMC surface are given in Scheme 1. The strong attraction between NNMC and PAA results the formation of an ultrathin uniform and PAA layer on NNMC. At the final thermal imidization process, the PAA layer is completely transformed to the PI layer instead of turning

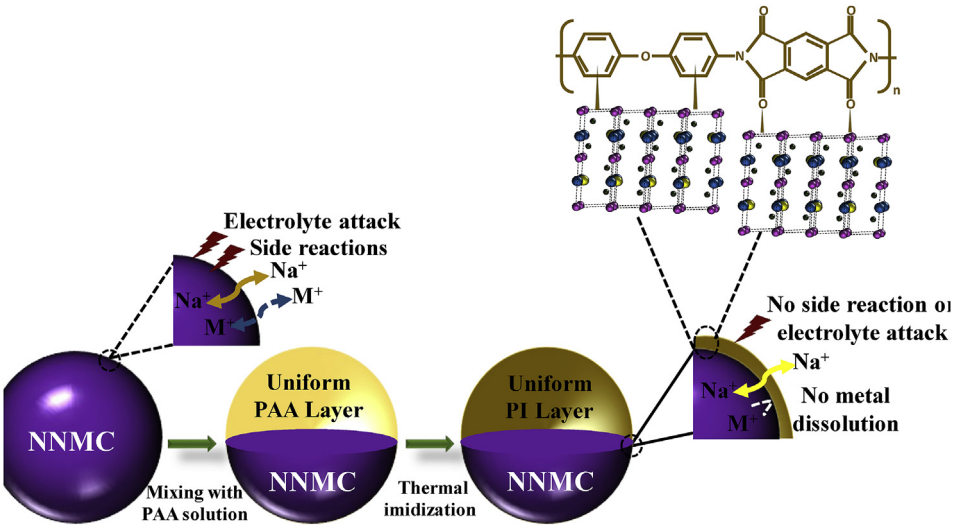

Scheme 1. Schematic representation of PI coating layer on NNMC materials.

into carbon layer as confirmed by Raman analysis. In addition, charge transfer reactions occur between the electron acceptors (Mn^{4+} in NNMC) and donors to form weak Mn (III)···O and Mn(III) …. benzene ring interaction as demonstrated by XPS, which favors the tight protective PI encapsulation against electrolyte attack and metal ion dissolution during the charge-discharge process and the resultant improvement of battery cycling stability [25]. The uniform PI layer with high ionic conductivity and thermal stability would also facilitate and stabilize the electrochemical reactions, which will be discussed in latter sections.

The CV of NNMC, Al-NNMC and PI-NNMC half cells are conducted against sodium metal anode between 2 and 4.5 V at 0.1 mV s^{-1} and presented in Fig. S6a. The CV traces reveal the complexity of electrochemical intercalation/deintercalation of Na-ions into the NNMC structures by showing three redox pairs corresponding to phase transformation during the positive and negative scans. Similar trend has been also reported for various P2 type layered materials containing multiple transition metal elements [27,59]. As seen in Fig. S6a, all the CV curves show redox peaks at ~ 4.3, 3.6 and 2.3 V, which could be assigned to the electrochemical redox reactions of $Ni^{2+/4+}$, $Co^{3+/4+}$ and $Mn^{3+/4+}$, respectively [29]. Ma et al. revealed that this complex electrochemical reaction nature of the layered materials could possibly result from the Na-ion vacancy ordering and the gliding of oxygen planes [60]. Fig. S6a

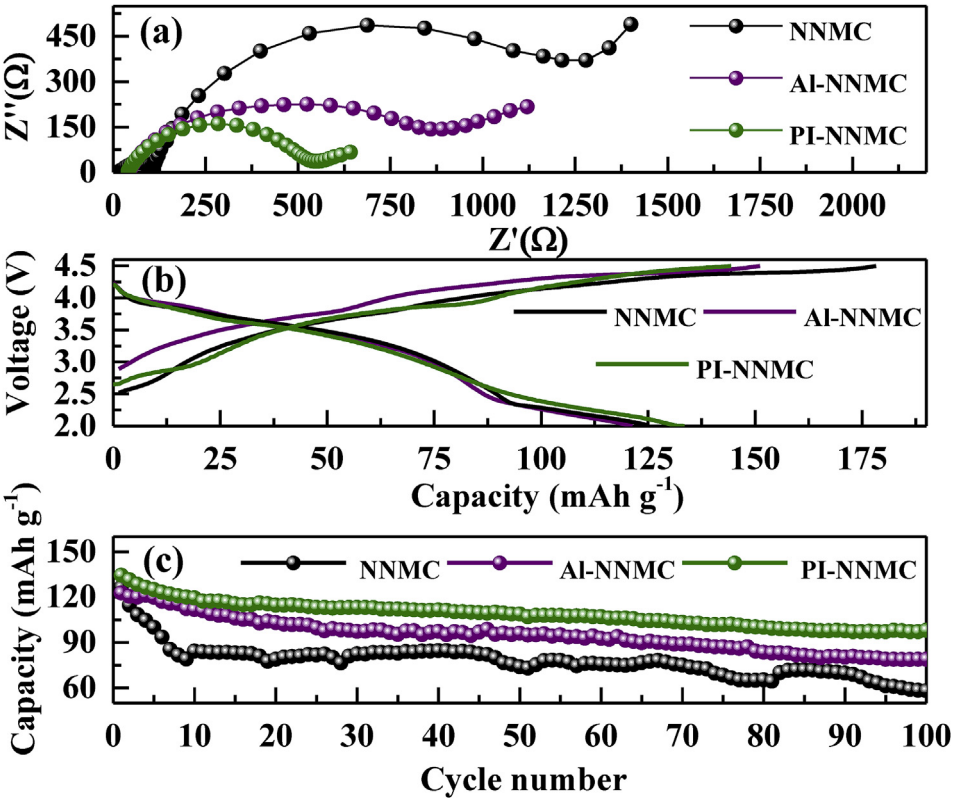

Fig. 4. (a) Nyquist plots of pristine and surface modified NNMC electrodes recorded at open circuit voltages; (b) C/DC and (c) cyclic stability of NNMC, Al-NNMC and PI-NNMC electrodes measured within 2–4.5 V at 1C rate.

Table 2
Electrochemical parameters of half cells containing NNMC, Al-NNMC and PI-NNMC cathodes before and after 100 cycles at 1C rates.

Sample name	Before cycles		First C/DC behaviors			After 100C/DC cycles			
	R_s (Ω)	R_{ct} (Ω)	Charge capacity	Discharge capacity	CE (%)	R_s (Ω)	R_{ct} (Ω)	Stability (%)	CE (%)
NNMC	109.5	1480.2	178.3	121.3	68	2757.5	3147.9	46	90.6
Al-NNMC	39.2	820.7	160.5	124.8	78	42.7	1003.4	70	96.7
PI-NNMC	39.7	477.5	164.2	151.6	92	17.2	545.3	81	98.4

clearly proves that the PI-NNMC/Na^+ cell exhibits a stronger current response than NNMC/Na^+ and Al-NNMC/Na^+ cells. Moreover, the NNMC electrode displays a peak shift towards lower potential during the negative scan as detected in Fig. 4a, which confirms the higher electrochemical polarization of Ni^{2+}/Ni^{4+} redox reaction and implies the restricted utilization of the active Ni species in the electrochemical reaction [40–42,57]. Hence, lower capacity and worse cycling performance would be expected from the sample without any coatings. The higher current response of PI-NNMC/Na^+ cell might be due to the uniformly distributed particles with enhanced ionic conductive properties and the presence of conductive N functional group on the surface of the particles [46,55].

The Nyquist plots of the cells recorded between 200 kHz and 100 mHz before cycling are illustrated in Fig. 4a and Fig. S6b (enlargement of Nyquist curves) and the corresponding impedance parameters are listed in Table 2. Generally, the intersection of a semicircle with real axis at the high frequency represents the contact/ohmic resistance (Rs), which associated with the ionic migration resistance. In Fig. 4a, the semicircle is composited of two parts in which the first semicircle at high frequency region denote the impedance corresponds to the interfacial resistance (i.e. R_{SEI}). The semicircle at medium frequency region is represented the faradaic charge transfer resistance (R_{ct}) at the interface and its double layer capacitance as well. The tail part at the low frequency end is representing the sodium ion diffusion control process. A small variation in R_s value observed for all the curves in Fig. 4a and Fig. S6b could be neglected, as the complex reaction mechanism of Na-ion present in electrolyte leads to poor contact between the conducting species in the electrolyte, resulting in a slight variation in R_s [21,33,61]. It can also been seen from Table 2 that the PI-NNMC based cell has smaller R_{ct} value than the cells with NNMC and Al-NNMC electrodes. The lower R_{ct} value of PI-NNMC is ascribed to the formation of nitrogen containing coating layer on particles, which improved the reaction kinetics thus enhancing the electrochemical performance. The large R_{ct} value of pristine materials could be attributed to the severe reaction of active species with carbonate-based electrolyte and subsequent byproducts (inorganic and polymeric) formation over the surface of the electrode [36]. This clearly revealed from Fig. 4a and Table 2 that the IPEL played an important role in increasing the Na-ion storage behavior of the NNMC material by alleviating the cell polarization, which would enhance cycling process at higher cut-off voltage [25].

The C/DC behaviors of the fabricated cells were conducted between 2 and 4.5 V at different current densities and the C/DC profiles of the cells cycled at 1C rate are given in Fig. 4b. As expected, the C/DC curves display three plateaus at ~2.3, 3.6 and 4.2 V within the recorded potential range, correlating well with the CV results [27]. Furthermore, the voltage profiles of PI-NNMC shows the longest discharge reaction plateau among the cells constructed, indicating the enhanced active material utilization attributed to the PI encapsulation [25,27,48]. It is reported that the thickness of PI coating layer should be controlled as thin as possible [48,58]. Previous reports clearly demonstrated that the larger decrease in ionic conductance could be observed from thicker PI coating on the surface [58]. The lower ionic conductance at high PI coating thickness is attributed to the larger ohmic polarization, which will become severer at high discharge current densities (for thicker PI coating). Therefore, we particularly controlled the PI coating thickness to be as thin as possible. The PI coating thickness was optimized at ~1.5 nm (data not shown), and this also exhibited better performance compared to the pristine and metal oxide coated NNMC electrode.

In addition, all the cells exhibit irreversible capacity losses (ICL) during the initial C/DC profile as seen from Fig. 4b. Generally, the ICL in the initial cycles is associated with the possible irreversible reactions such as decomposition of the electrolyte, which results in the formation of a SEI [21,35]. The first charge and discharge capacities as well as the Coulombic efficiency (CE) values of all cells are listed in Table 2. Discharge capacities of 126.3, 127.8 and 133.16 mAh g^{-1} could be obtained from NNMC, Al-NNMC and PI-NNMC electrode, respectively at 1C rate between 2 and 4.5 V. Although all the fabricated cells show ICL during the first cycle, the cells with Al_2O_3 and PI coated NNMC electrodes show improved initial CE of 78 and 92%, respectively, compared to the pristine electrode (68%). This clearly reveals that the irreversible intercalation/deintercalation of Na-ions in NNMC structure and the detrimental side reactions at electrode/electrolyte interface are effectively alleviated by the ultrathin encapsulation of coating materials [33]. Moreover, it is widely known that the PI has excellent ionic conductivity compared to metal oxide coatings [48,50,58]. Due to the uniform and ultrathin coverage (~1.5 nm) of PI on the NNMC surface, the impact on cell resistance due to encapsulation is mitigated as confirmed by EIS measurements (Fig. 4a), and the PI-NNMC electrode retains good ion conduction for satisfactory discharge capacity [46].

To further understand the electrochemical process of NNMC, Al-NNMC and PI-NNMC electrodes, the differential capacity plots (dQ/dV) are drawn from the initial C/DC curves and the corresponding dQ/dV plots are presented in Fig. S6c. There are three clear oxidation and reduction peaks at ~4.3, 3.6 and 2.3 V corresponding to the $Ni^{2+/4+}$, $Co^{3+/4+}$ and $Mn^{3+/4+}$, redox couple, respectively in Fig. S6c [21]. This is well agreed with the CV and C/DC results as shown in Fig. 4. In addition, a new anodic peak can be noted at 3.29 V (insert in Fig. S6c), which is associated to the newly formed Mn(III). On the other hand, a peak at ~3.30 V observed during discharge can be assigned to the reduction of Mn(IV) to Mn(III) [25,38]. The cycling performances of the pristine and surface modified electrodes are presented in Fig. 4c. The pristine NNMC electrode delivers an initial capacity discharge capacity of ~126 mA h^{-1} at 1C rate and shows severe capacity decay until the tenth cycle. The capacity retention after 25th cycle is about 65% with a capacity of 82 mAh g^{-1}. Irreversible capacity fade is commonly observed in high-voltage SIBs, with the primary reason attributed to a reversible P2-O2 phase transition via an intermediate OP4 phase [40]. This phase change is ascribed to higher coulombic repulsion of the adjacent oxygen layer when more Na-ions are extracted from the structure at high potential operation, which is confirmed by *in situ/ex situ* XRD measurement elsewhere [27,62].

There are several other reasons also responsible for the capacity fade during the initial cycles including (i) formation of SEI layer from electrolyte decomposition, (ii) active species dissolution in to the electrolyte, (iii) severe internal stress due to the larger Na-ion accommodation, and (iv) incorporation of solvated ions into the metal oxide matrix [27,40–42,62]. Hence, the capacity of pristine electrode is found to decrease gradually with the capacity retention of 46% after 100 cycles. Considering that many factors that affect the stability of P2-type materials at high potential region as described above, surface modification is a good strategy to enhance the interfacial properties by eliminating the direct contact of electrode materials with the electrolyte.

The cycling performance comparison in Fig. 4c clearly demonstrates that the presence of coating layers (PI or Al_2O_3) has significant impact in

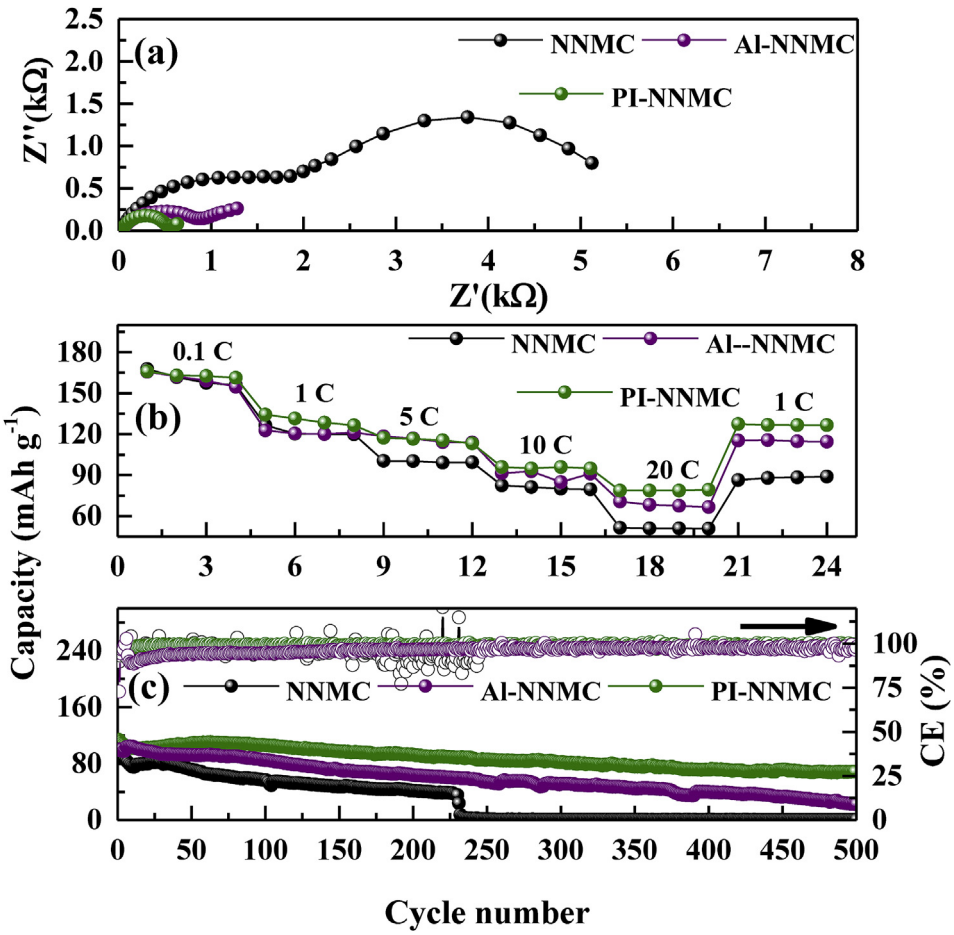

Fig. 5. (a) Impedance spectrum of NNMC, Al- NNMC and PI- NNMC recorded after 100C/DC cycles, (b) rate performance of pristine and surface modified NNMC electrodes at difference current rates within 2–4.5 V and (c) long term cyclability of NNMC, Al- NNMC and PI- NNMC electrodes tested at 5C rates.

improving the stability of pristine NNMC at high cut-off voltage range. In addition, the smooth C/DC curves of Al-NNMC and PI-NNMC electrodes in Fig. 4b further confirm the suppression of the irreversible P2-O2 phase transition above 4.25 V. Moreover, the cyclic performances in Fig. 4c also show significantly smaller initial capacity fade for the coated electrodes, confirming the enhancement of the interfacial properties of pristine NNMC electrode by uniform thin coating layer. The enhanced cyclic stability of Al_2O_3 coated electrode is mainly related to the large band gap energy difference between the alumina and NNMC materials [41,42,57]. It was reported that the electrons in the conduction band of the cathode material move into the coating materials during C/DC and undergoes a redox reaction if the band gap energy is relatively low [41,57]. This would greatly affect the electrochemical stability of the parent materials and hence the selection of coating material with large band gap is essential [38]. The Al_2O_3 has a higher band gap energy (~9 eV) than other known coating materials ($ZrO_2 = 5.8$ eV and $TiO_2 = 3.18$ eV), which makes it a promising candidate to enhance the electrochemical cycling performance [41,57,63]. On the other hand, PI-NNMC electrode shows significantly enhanced cyclic performance compared with pristine and Al_2O_3 coated NNMC cathode. Fig. 4c confirms that the half-cell fabricated with PI-NNMC maintains ~81% of its initial discharge capacity, which is higher than NNMC (~46%) and Al-NNMC (~70%) cathode after 100 cycles. To understand the impact of coating layer on the electrochemical stability, the EIS measurements were conducted on NNMC, Al-NNMC and PI-NNMC cells and the impedance parameters are summarized in Table 2. As seen from Table 2 and Fig. 5a, the R_{ct} value of pristine electrode dramatically increased from 1480.2 Ω to 3147.9 Ω after 100 cycles. This validates that the severe capacity decay of pristine NNMC electrode could be ascribed to the undesirable interfacial side reaction with the harmful electrolyte [27,35]. The formed resistive layer hinders the charge transportation at SEI layer and thereby deteriorates the sodium ion storage behavior at high voltage operation. In comparison, the surface modified cathodes, particularly PI-NNMC cathode, has a slightly increased R_{ct} value after 100 cycles, effectively eliminating the formation of resistive layer by preventing direct exposure of charged NNMC electrode to the acidic electrolyte [27]. It is noteworthy here that the PI-NNMC/Na half-cell displays the lowest R_{ct} value among all the sample cells as shown in Table 2, which could be a solid evidence for the excellent cyclic behavior of PI-NNMC electrode. In addition, PI is well known as a good ion conductor, the coating of which on NNMC could improve the ion conduction at the electrode/electrolyte interface to improve reaction kinetics and reversibility. Consequently, the robust PI encapsulation favors the stabilization of the parent material at high voltage range and thus contribute to enhanced electrochemical performance [58,64].

The rate capability of the NNMC, Al-NNMC and PI-NNMC electrodes were analyzed between 2 and 4.5 V at current densities from 0.1C to 20C (1C = 160 mA h g^{-1}). As seen from Fig. 5b, the surface modified cathodes show slightly improved rate performance at all current densities. It is well known that electrode materials undergo severe stress and strain during the C/DC studies at high current rates, which can be mitigated by the surface protection [34,38]. The enhanced rate performance of the surface modified cathodes could be attributed to the following reasons but not limiting to (i) the surface modification promotes the ionic transport from cathode to current collector [40], (ii) the surface coating decreases the activation energy for charge transfer at SEI layer [65], and (iii) the coating layer assists to eliminate inherent mechanical stress during high current cycling process, retaining the structural and electrochemical

Table 3
ICP results of pristine and surface modified materials chocked in electrolyte for 7 days at 40 °C.

Sample	Mn dissolution (ppm)	Co dissolution (ppm)	Ni dissolution (ppm)
NNMC	113.339	31.327	32.5698
Al-NNMC	0.019	0.0019	0.0014
PI-NNMC	0.0093	0.0012	0.0011

behaviors especially at high cut-off voltages [66]. Another reason of the excellent rate capabilities of PI-NNMC electrode could be also probably ascribed to the partial reduction of Mn (as confirmed in XPS) [48,52,58]. Since the presence of one type of metal ion at different valency states (Mn^{3+} and Mn^{4+}) has been proposed to facilitate the polarons movement, the appearance of Mn^{3+} after PI coating is likely responsible for enhancing the discharge capacity value of PI-NNMC under high current [67,68].

Although both Al_2O_3 and PI-encapsulated cathodes display very close capacities at lower current rates (0.1–10C), a predominant difference in discharge capacities could be observed at high current rate. For instance, the Al-NNMC/Na^+ cell displays a discharge capacity of 70 mAh g^{-1} at 20C rate (3.2 A g^{-1}) whereas the half-cell containing PI-NNMC electrode has 80 mAh g^{-1} at the same testing condition. Moreover, when the current is reverted to 1C, the discharge capacity of the PI-NNMC electrode recovers to 127 mAh g^{-1} whereas the pristine NNMC, Al-NNMC electrodes only retains 86.4 and 115.7 mAh g^{-1}, respectively. The enhanced rate performance of PI-NNMC clearly reveals that the severe reactivity of parent material with electrolyte counterpart and subsequent formation of inorganic and polymeric by-product on the electrode is significantly eliminated by developing simple polymer coating [27]. Thus, the increased electrochemical behavior in terms of high stability and rate performance are realized for PI-NNMC materials at high current and voltage operation [69].

In addition to the tremendous rate performance, long term cyclabilities of NNMC, PI-NNMC and Al-NNMC electrodes at 5C rate are presented in Fig. 5c. As seen in Fig. 5c, the pristine electrode shows almost no capacity retained after 225 cycles while Al-NNMC electrode has 20% retention after 500 cycles at 5C rate. On the other hand, PI-NNMC retains nearly 70% of the initial capacity value under the same conditions. High rate capability along with extended cycle life at high operating voltage are important parameters for large scale energy storage devices, as we demonstrate here on a sodium ion battery. The discharge capacity and cycling stability of the as-developed PI-NNMC electrode at high current exceed many reports based on P2 layered cathodes and to the best of our knowledge, has never been reported on sodium-based P2 type layered materials cycled >4.3 V [19,20,29–31,35–42,70–73]. The discharge capacity, current rate, and cycle retention of numerous P2 layered materials tested at high cut-off voltages (>4.25 V, voltage range given in the bracket) were compared with PI-NNMC materials and the corresponding graphs are illustrated in Figs. S7a and S7b, respectively [37–39].

To evaluate the metal dissolution inhibition behavior of coating layer, the NNMC, Al-NNMC and PI-NNMC powders were stored in the electrolyte for 7 days at 40 °C. The ICP analysis was employed to examine the amount of metal leaching by the electrolyte and the results are presented in Table 3. It is apparent that the metal dissolution is severe for NNMC electrode, while the surface modified materials exhibit much lower metal dissolution (Al-NNMC > PI-NNMC). This further confirms that the surface modification (Al or PI) effectively hinders the electrolyte attack and thereby minizine the dissolution of active materials into the electrolyte, which is essential to maintain excellent electrochemical stability for long term cycling. Apart from the surface protection, the PI layer also has great impact on the thermal stability, which is evaluated by DSC analysis. The DSC thermograms of pristine and surface modified material are presented in Fig. S8a. In general, the reduction of total heat generated by the side reaction or the exothermic peak shift towards higher temperature value is an good indication of thermally stabilized interface between SEI layer [52]. The DSC thermograms in Fig. S8a demonstrates that the PI-NNMC displays low exothermic heat (low peak intensity) and clear peak shift to

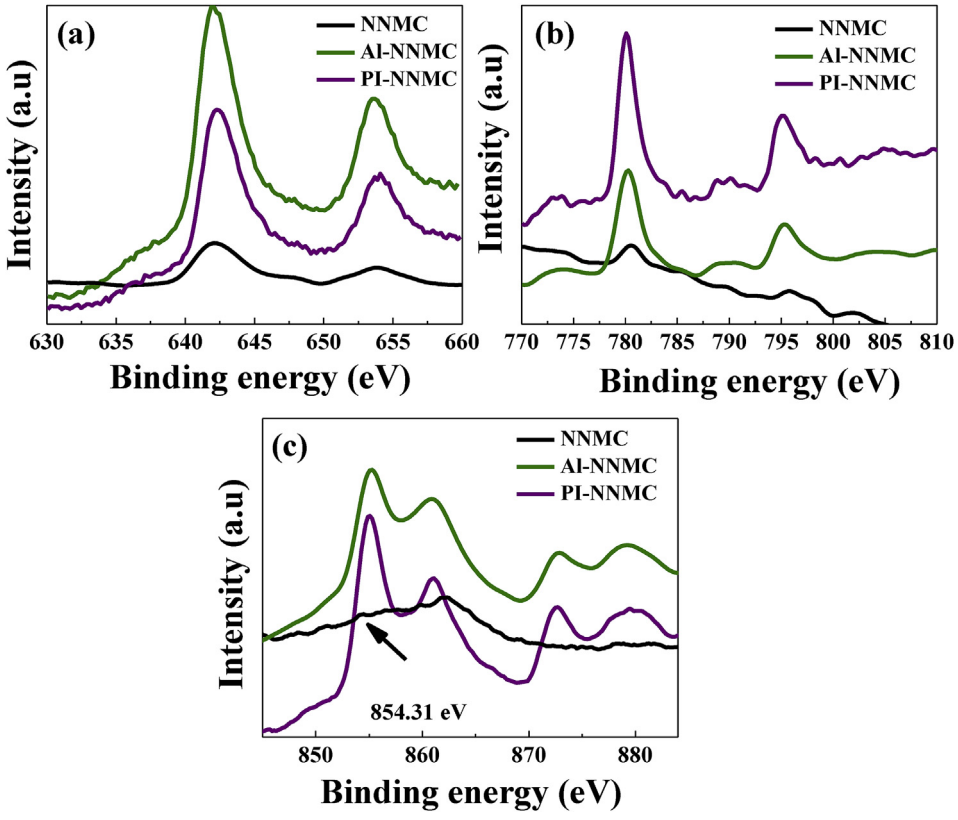

Fig. 6. XPS spectra of (a) Mn 2p (b) Co 2p and (c) Ni 2p of NNMC and surface modified NNMC after 500 cycling process.

high exothermic peak temperature ($T_{peak} = 280\,^{\circ}C$) than pristine and alumina coated NNMC. The DSC results show that the PI layer provides excellent surface coverage and successfully prevents direct contact of NNMC with the acidic electrolyte, which sequentially alleviates the interfacial exothermic reaction between the active species and harmful electrolyte at the higher cut-off voltages. A schematic representation of the role of PI encapsulation in increasing thermal stability of pristine NNMC, as compared to the Al-NNMC, is given in Fig. S8b.

Changes in the surface valence of the active species before and after cycling process were investigated using *ex situ* XPS. It is apparent in Fig. 5c that the NNMC electrode is dead after 225 cycles but the Al-NNMC and PI-NNMC electrodes can be C/DC for 500 cycles at higher rates (5C). Hence, all cells were opened after 500 cycles to extract the electrode for XPS studies. The electrodes were washed with DEC and dried under vacuum for 24 h before the XPS analysis. The XPS spectrums of Ni 2p, Mn 2p and Co 2p after cycling are presented in Fig. 6 and the corresponding main peak positions are listed in Table 4 along with the respective peak positions obtained before cycling process. As shown in Table 4, the peak positions of Mn 2p for all samples does not change much after cycles, inferring that the local structure around the Mn atoms does not vary greatly after cycling and that the Mn ions existed mostly in Mn^{4+} state. However, Co 2p of NNMC sample clearly displays peak shift towards higher energy levels after cycles while surface modified NNMC electrode does not exhibit any changes in peak position. This demonstrates that the valence state of Co ions after cycles retained at +3 for surface modified samples and the local structural distortion in Co-O6 octahedra is occurred for unprotected NNMC sample [24,25].

In contrast to the Mn and Co spectra, the Ni 2p spectrum of NNMC electrode after cycles in Fig. 6c shows clear differences in peak position and intensities. After cycling, the Ni element becomes weakened and shifts to lower energy (854.31 eV). The disappearance of major characteristic peaks of Ni 2p reveals the dissolution of Ni active species into the electrolyte, which significantly affects its electrochemical performance. Severe capacity decay is more obvious for the unprotected electrode at high voltage cycling because of the harmful reaction with the electrolyte and the subsequent dissolution of active species [25]. In addition, the peak shift towards lower energy further confirms that the oxidation state of Ni in NNMC electrode could not retain the oxidation state of +2 after C/DC studies. It is clear from Fig. 5c that the NNMC cell almost failed after 225 cycles at 5C rate due to the dissolution of electrode materials into the acidic electrolyte and the local structural distortion during C/DC cycles. On the other hand, the peak position of Ni 2p for Al-NNMC and PI-NNMC electrode are unchanged compared to those before cycling, concluding that the redox reaction of $Ni^{2+/4+}$ couple is more reversible. To confirm this phenomenon, the C/DC profiles of NNMC, Al-NNMC and PI-NNMC after 225 cycles at 5C are presented in Fig. S8a further to demonstrate the role of the surface modification in protecting the active species in NNMC electrodes. It is clear that the shape C/DC profile of Al-NNMC and PI-NNMC are almost identical and still exhibit the redox plateaus of Ni, Mn and Co at respective voltages, whereas the $Ni^{2+/4+}$ redox plateau in NNMC electrode can be barely observed at 4.3 V. This reveals the severe side reaction and dissolution of active species into the electrolyte, thus the performance of the parent materials fades after 225 cycles. Therefore, the surface modification is not only protecting the electrode surface from the acidic acid attack, but also stabilizes SEI formation after the cycling process to achieve long term stability. This justification agrees well with the results obtained from the EIS, C-DC at different currents and the long-term cycling as shown in Fig. 5.

Although surface modifications have improved the stability of pristine NNMC electrode, the alumina and PI coated NNMC delivers different C-DC performances. The reason behind the difference in performances is also examined using XPS studies after 500 cycles at 5C rate and the corresponding Al 2p and N 1s spectra of Al-NNMC and PI-NNMC, respectively are given in Fig. S8. The Al 2p spectra of Al-NNMC after 500 cycles in Fig. S9b shows a peak around at 75.6 eV, which is higher than that observed before cycling process (74.4 eV) but closer to that reported for Al-OH (75.1 eV) [74]. This data implies that the Al_2O_3 coating layer might have reacted with the electrolyte/cathode counterparts during the subsequent cycling to form byproduct and thus affects the electrochemical performance [75]. On the other hand, the N 1s spectra of PI-NNMC electrode (Fig. S9c) remains unchanged at 400.27 eV before (Fig. 1e) and after cycles and the peak is mainly associated to the amine group (C-NH_2) [76,77]. These results indicate that the PI coating is more stable in electrolyte than Al_2O_3 and can persistently perform the surface protection and conductivity enhancement for NNMC. To correlate this statement, the EIS spectra of AI-NNMC and PI-NNMC were taken after 500 cycles at 5C rate and their Nyquist plots are presented in Fig. S9d. As shown in Fig. S9d, NNMC electrode coated with PI has lower charge transfer resistance than Al-NNMC electrode after 500 cycles, implying the improved conductive properties of PI coated NNMC electrode. Thus, stable and prolonged cyclic performance are achieved from PI-NNMC. This PI coating strategy certainly provides an effective method to enhance the electrochemical stability of P2 layered cathode materials at high cut-off voltage cycling by employing a simple polymer encapsulation, which can be easily extended for other sodium-based energy sources.

Table 4
XPS peak positions of Ni, Co and Mn 2p spectra before and after cycles. The measurement taken after 250 cycles at 1C for NNMC electrode while the XPS performance on Al-NNMC and PI-NNMV after 500 cycles at 5C rate.

Sample name	Mn 2p (eV)		Co 2p (eV)		Ni 2p (eV)	
	Before cycles	After cycles	Before cycles	After cycles	Before cycles	After cycles
NNMC	642.61	642.35	780.32	780.53	854.91	854.31
Al-NNMC	642.61	642.26	780.32	780.28	854.91	855.01
PI-NNMC after	641.90	642.01	780.32	780.32	854.91	855.01

4. Conclusion

An ion-conductive polymer electrolyte (polyimide, PI) encapsulation on $Na_{2/3}(Mn_{0.54}Ni_{0.13}Co_{0.13})O_2$ (NNMC) surface has been employed to enhance the electrochemical cycling stability at high potential range beyond > 4.3 V for the first time. The electrochemical performances including stability and rate capability of NNMC have been significantly improved after PI surface coating compared with pristine and alumina (Al_2O_3) coated NNMC electrodes. The PI-NNMC exhibits excellent capacity retention of ~70% after 500 cycles at 5C while pristine and alumina coated NNMC shows much lower cyclic stability. This high rate stability is attributed to a slight shift of Mn valence state (Mn^{4+} to Mn^{3+}) after PI coating as confirmed by XPS study, which is beneficial for the migration of polarons and enhances the performances at high current rates. In addition, the interfacial exothermic reaction between NNMC and acidic electrolyte is also successfully alleviated by the PI layer. These results demonstrate that the PI ion-conductive protective layer plays a vital role in facilitating and stabilizing the redox reactions during the cyclic process on high voltage cathodes, which is important to fabricate large scale battery packs for electric vehicles.

Acknowledgements

This work was financially supported by the Natural Sciences and Engineering Research Council of Canada, the University of Waterloo, and the Waterloo Institute for Nanotechnology, University of Waterloo and the 111 Project (No. D17007) and K.K acknowledges the financial support for this work from Henan Normal University, China.

Appendix A. Supplementary data

Supplementary data to this article can be found online at https://doi.org/10.1016/j.ensm.2019.07.010.

References

[1] V. Etacheri, R. Marom, R. Elazari, G. Salitra, D. Aurbach, Energy Environ. Sci. 4 (2011) 3243–3262.
[2] G.H. Newman, L.P. Klemann, J. Electrochem. Soc. 127 (1980) 2097–2099.
[3] K.M. Abraham, Solid State Ion. 7 (1982) 199–212.
[4] Y. Wang, W. Zhu, A. Guerfi, C. Kim, K. Zaghib, Front. Energy Res. 7 (2019).
[5] W. Luo, F. Shen, C. Bommier, H. Zhu, X. Ji, L. Hu, Acc. Chem. Res. 49 (2016) 231–240.
[6] Y. Liang, W.-H. Lai, Z. Miao, S.-L. Chou, Small 14 (2018) 1702514.
[7] D. Xu, C. Chen, J. Xie, B. Zhang, L. Miao, J. Cai, Y. Huang, L. Zhang, Adv. Energy Mater. 6 (2016) 1501929.
[8] W. Ma, K. Yin, H. Gao, J. Niu, Z. Peng, Z. Zhang, Nano Energy 54 (2018) 349–359.
[9] W. Ma, J. Wang, H. Gao, J. Niu, F. Luo, Z. Peng, Z. Zhang, Energy Storage Mater. 13 (2018) 247–256.
[10] W.P. Kalisvaart, B.C. Olsen, E.J. Luber, J.M. Buriak, ACS Appl. Energy Mater. 2 (2019) 2205–2213.
[11] D. Wu, X. Li, B. Xu, N. Twu, L. Liu, G. Ceder, Energy Environ. Sci. 8 (2015) 195–202.
[12] P. Senguttuvan, G. Rousse, V. Seznec, J.-M. Tarascon, M.R. Palacín, Chem. Mater. 23 (2011) 4109–4111.
[13] C. Chen, H. Xu, T. Zhou, Z. Guo, L. Chen, M. Yan, L. Mai, P. Hu, S. Cheng, Y. Huang, J. Xie, Advanced Energy Materials 6 (2016) 1600322.
[14] C. Chen, Y. Wen, X. Hu, X. Ji, M. Yan, L. Mai, P. Hu, B. Shan, Y. Huang, Nat. Commun. 6 (2015) 6929.
[15] M.D. Slater, D. Kim, E. Lee, C.S. Johnson, Adv. Funct. Mater. 23 (2013) 947–958.
[16] M. Tamaru, S.C. Chung, D. Shimizu, S.-i. Nishimura, A. Yamada, Chem. Mater. 25 (2013) 2538–2543.
[17] K. Kaliyappan, Z. Chen, J. Electrochem. Soc. 165 (2018) A1822–A1828.
[18] K. Kaliyappan, Z. Chen, Electrochim. Acta 283 (2018) 1384–1389.
[19] R. Berthelot, D. Carlier, C. Delmas, Nat. Mater. 10 (2011) 74–80.
[20] N. Yabuuchi, M. Kajiyama, J. Iwatate, H. Nishikawa, S. Hitomi, R. Okuyama, R. Usui, Y. Yamada, S. Komaba, Nat. Mater. 11 (2012) 512–517.
[21] A. Caballero, L. Hernan, J. Morales, L. Sanchez, J. Santos Pena, M.A.G. Aranda, J. Mater. Chem. 12 (2002) 1142–1147.
[22] C. Delmas, J.J. Braconnier, C. Fouassier, P. Hagenmuller, Solid State Ion. 3–4 (1981) 165–169.
[23] M. Guignard, C. Didier, J. Darriet, P. Bordet, E. Elkaïm, C. Delmas, Nat. Mater. 12 (2013) 74–80.
[24] V. Palomares, P. Serras, I. Villaluenga, K.B. Hueso, J. Carretero-Gonzalez, T. Rojo, Energy Environ. Sci. 5 (2012) 5884–5901.
[25] V. Palomares, M. Casas-Cabanas, E. Castillo-Martinez, M.H. Han, T. Rojo, Energy Environ. Sci. 6 (2013) 2312–2337.
[26] D.H. Lee, J. Xu, Y.S. Meng, Meet. Abstr. MA2012-02 (2012) 1842.
[27] Z. Lu, J.R. Dahn, J. Electrochem. Soc. 148 (2001) A1225–A1229.
[28] D. Buchholz, A. Moretti, R. Kloepsch, S. Nowak, V. Siozios, M. Winter, S. Passerini, Chem. Mater. 25 (2012) 142–148.
[29] D. Yuan, W. He, F. Pei, F. Wu, Y. Wu, J. Qian, Y. Cao, X. Ai, H. Yang, J. Mater. Chem. 1 (2013) 3895–3899.
[30] H. Yoshida, N. Yabuuchi, K. Kubota, I. Ikeuchi, A. Garsuch, M. Schulz-Dobrick, S. Komaba, Chem. Commun. 50 (2014) 3677–3680.
[31] K. Park, D. Han, H. Kim, W.-s. Chang, B. Choi, B. Anass, S. Lee, RSC Adv. (2014), https://doi.org/10.1039/C4RA01391C.
[32] K. Karthikeyan, S. Amaresh, S.H. Kim, V. Aravindan, Y.S. Lee, Electrochim. Acta 108 (2013) 749–756.
[33] K. Karthikeyan, S. Amaresh, G.W. Lee, V. Aravindan, H. Kim, K.S. Kang, W.S. Kim, Y.S. Lee, Electrochim. Acta 68 (2012) 246–253.
[34] S.K. Jeong, C.-H. Song, K.S. Nahm, A.M. Stephan, Electrochim. Acta 52 (2006) 885–891.
[35] D. Yuan, X. Hu, J. Qian, F. Pei, F. Wu, R. Mao, X. Ai, H. Yang, Y. Cao, Electrochim. Acta 116 (2014) 300–305.
[36] L. Wang, Y.-G. Sun, L.-L. Hu, J.-Y. Piao, J. Guo, A. Manthiram, J. Ma, A.-M. Cao, J. Mater. Chem. 5 (2017) 8752–8761.
[37] J.-Y. Hwang, S.-T. Myung, Y.-K. Sun, Chem. Soc. Rev. 46 (2017) 3529–3614.
[38] X. Gui-Liang, A. Rachid, A. Ali, C. Haiying, D. Mouad, M. Zi-Feng, S. Ismael, A. Jones, M.W. Liu, P. Feng, C. Zonghai, A. Khalil, Advanced Energy Materials 8 (2018) 1702403.
[39] Y. Ya, M. Arumugam, Advanced Energy Materials 8 (2018) 1701785.
[40] H.V. Ramasamy, K. Kaliyappan, R. Thangavel, V. Aravindan, K. Kang, D.U. Kim, Y. Park, X. Sun, Y.-S. Lee, J. Mater. Chem. (2017), https://doi.org/10.1039/C6TA10334K.
[41] K. Kaliyappan, J. Liu, B. Xiao, A. Lushington, R. Li, T.-K. Sham, X. Sun, Adv. Funct. Mater. 27 (2017), 1701870-n/a.
[42] K. Kaliyappan, J. Liu, A. Lushington, R. Li, X. Sun, ChemSusChem 8 (2015) 2537–2543.
[43] T.O. Magu, A.U. Agobi, L. HITLER, P.M. Dass, J. Chem. Rev. 1 (2019) 19–34.
[44] K. Karthikeyan, S. Amaresh, V. Aravindan, W.S. Kim, K.W. Nam, X.Q. Yang, Y.S. Lee, J. Power Sources 232 (2013) 240–245.
[45] K. Karthikeyan, S. Amaresh, V. Aravindan, H. Kim, K.S. Kang, Y.S. Lee, J. Mater. Chem. 1 (2013) 707–714.
[46] J. Zhang, Q. Lu, J. Fang, J. Wang, J. Yang, Y. NuLi, ACS Appl. Mater. Interfaces 6 (2014) 17965–17973.
[47] Z. Song, H. Zhan, Y. Zhou, Angew. Chem. 122 (2010) 8622–8626.
[48] J.-H. Park, J.-S. Kim, E.-G. Shim, K.-W. Park, Y.T. Hong, Y.-S. Lee, S.-Y. Lee, Electrochem. Commun. 12 (2010) 1099–1102.
[49] J.-H. Park, J.-H. Cho, S.-B. Kim, W.-S. Kim, S.-Y. Lee, S.-Y. Lee, J. Mater. Chem. 22 (2012) 12574–12581.
[50] Y.K. Lee, J.D. Craig, in: Polymer Materials for Electronic Applications, vol. 184, AMERICAN CHEMICAL SOCIETY, 1982, pp. 107–121, ch. 9.
[51] L.Y. Jiang, Y. Wang, T.-S. Chung, X.Y. Qiao, J.-Y. Lai, Prog. Polym. Sci. 34 (2009) 1135–1160.
[52] J.-H. Cho, J.-H. Park, M.-H. Lee, H.-K. Song, S.-Y. Lee, Energy Environ. Sci. 5 (2012) 7124–7131.
[53] H. Banda, D. Damien, K. Nagarajan, M. Hariharan, M.M. Shaijumon, J. Mater. Chem. 3 (2015) 10453–10458.
[54] K. Karthikeyan, S. Amaresh, S.N. Lee, X. Sun, V. Aravindan, Y.G. Lee, Y.S. Lee, ChemSusChem 7 (2014) 1435–1442.
[55] C.C. Li, H. Yu, Q. Yan, H.H. Hng, Electrochim. Acta 187 (2016) 406–412.
[56] M.C. Biesinger, B.P. Payne, L.W.M. Lau, A. Gerson, R.S.C. Smart, Surf. Interface Anal. 41 (2009) 324–332.
[57] K. Kaliyappan, Z. Chen, Nano Energy 48 (2018) 107–116.
[58] J.-H. Park, J.-H. Cho, E.-H. Lee, J.-M. Kim, S.-Y. Lee, J. Power Sources 244 (2013) 442–449.
[59] M. Sathiya, K. Hemalatha, K. Ramesha, J.M. Tarascon, A.S. Prakash, Chem. Mater. 24 (2012) 1846–1853.
[60] X. Ma, H. Chen, G. Ceder, J. Electrochem. Soc. 158 (2011) A1307–A1312.
[61] P. Suresh, A.K. Shukla, N. Munichandraiah, Mater. Lett. 59 (2005) 953–958.
[62] H. Wang, B. Yang, X.-Z. Liao, J. Xu, D. Yang, Y.-S. He, Z.-F. Ma, Electrochim. Acta 113 (2013) 200–204.
[63] H. Zhang, Z. Ji, T. Xia, H. Meng, C. Low-Kam, R. Liu, S. Pokhrel, S. Lin, X. Wang, Y.-P. Liao, M. Wang, L. Li, R. Rallo, R. Damoiseaux, D. Telesca, L. Mädler, Y. Cohen, J.I. Zink, A.E. Nel, ACS Nano 6 (2012) 4349–4368.
[64] D.J. Lee, M.-H. Ryou, J.-N. Lee, B.G. Kim, Y.M. Lee, H.-W. Kim, B.-S. Kong, J.-K. Park, J.W. Choi, Electrochem. Commun. 34 (2013) 98–101.
[65] H. Zhao, L. Gao, W. Qiu, X. Zhang, J. Power Sources 132 (2004) 195–200.
[66] X. Meng, X.-Q. Yang, X. Sun, Adv. Mater. 24 (2012) 3589–3615.
[67] H. Bordeneuve, S. Guillemet-Fritsch, A. Rousset, S. Schuurman, V. Poulain, J. Solid State Chem. 182 (2009) 396–401.
[68] A. Abouimrane, O.C. Compton, H. Deng, I. Belharouak, D.A. Dikin, S.T. Nguyen, K. Amine, Electrochem. Solid State Lett. 14 (2011) A126–A129.
[69] M.C. Kim, S.H. Kim, V. Aravindan, W.S. Kim, S.Y. Lee, Y.S. Lee, J. Electrochem. Soc. 160 (2013) A1003–A1008.
[70] X. Wu, J. Guo, D. Wang, G. Zhong, M.J. McDonald, Y. Yang, J. Power Sources 281 (2015) 18–26.
[71] Y. Wang, R. Xiao, Y.-S. Hu, M. Avdeev, L. Chen, Nat. Commun. 6 (2015).
[72] S. Bao, S. Luo, Z. Wang, Q. Wang, A. Hao, Y. Zhang, Y. Wang, J. Power Sources 362 (2017) 323–331.
[73] M.J. Aragón, P. Lavela, G. Ortiz, R. Alcántara, J.L. Tirado, J. Alloy. Comp. 724 (2017) 465–473.
[74] A. Nylund, I. Olefjord, Surf. Interface Anal. 21 (1994) 283–289.
[75] J. Liu, A. Manthiram, Chem. Mater. 21 (2009) 1695–1707.
[76] Z. Wang, Y. Dong, H. Li, Z. Zhao, H. Bin Wu, C. Hao, S. Liu, J. Qiu, X.W. Lou, Nat. Commun. 5 (2014) 5002.
[77] Y. Jiang, M. Wei, J. Feng, Y. Ma, S. Xiong, Energy Environ. Sci. 9 (2016) 1430–1438.